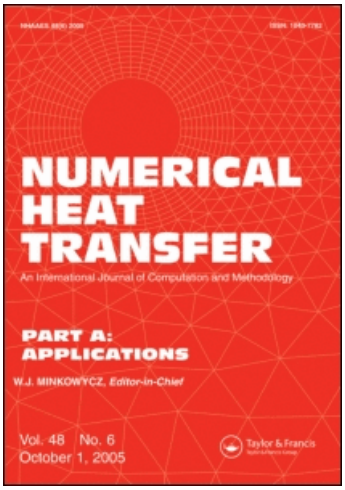

Numerical Heat Transfer, Part A: Applications
Publication details, including instructions for authors and subscription information:
http://www.informaworld.com/smpp/title~content=t713657973

SPATIOTEMPORAL STRUCTURES OF BUOYANCY-INDUCED FLOW IN A VERTICAL CHANNEL

H. Gunes [a]; R. A. Sahan [a]; A. Liakopoulos [a]
[a] Department of Mechanical Engineering and Mechanics, Lehigh University, Bethlehem, Pennsylvania, USA

To cite this Article Gunes, H., Sahan, R. A. and Liakopoulos, A.(1997) 'SPATIOTEMPORAL STRUCTURES OF BUOYANCY-INDUCED FLOW IN A VERTICAL CHANNEL', Numerical Heat Transfer, Part A: Applications, 32: 1, 51 — 62
To link to this Article: DOI: 10.1080/10407789708913879
URL: http://dx.doi.org/10.1080/10407789708913879

SPATIOTEMPORAL STRUCTURES OF BUOYANCY-INDUCED FLOW IN A VERTICAL CHANNEL

H. Gunes, R. A. Sahan, and A. Liakopoulos
Department of Mechanical Engineering and Mechanics, Lehigh University, Bethlehem, Pennsylvania 18015-3085, USA

The present investigation deals with the development of low-order representations of transitional free convection in a vertical channel with discrete heaters. The governing equations are solved using a spectral element method. Proper orthogonal decomposition (POD) is applied to extract the most energetic eigenfunctions (and the related spatiotemporal structures) from time-dependent numerical solutions of the full model equations at a Grashof number higher than the critical value. Using the computed eigenfunctions in a truncated series expansion, reconstruction of the original flow and temperature fields is achieved in an optimal way. It is found that almost all the flow and temperature fluctuation energy is captured by the first six eigenmodes. A low-dimensional set of nonlinear ordinary differential equations that describes the dynamics of the flow and temperature fields is also derived. It is found that low-order models based on retaining at least four eigenmodes for each field predict stable, self-sustained oscillations with correct amplitude and frequency.

INTRODUCTION

Low-dimensional modeling of convective flows is highly desired, since direct numerical simulations of transitional and turbulent convective flows require tremendous amounts of computational time and power. By obtaining accurate, low-order approximations to the full model (continuity, Navier-Stokes, and energy equations), a parametric study of such flows can be easily performed. In addition, low-order models are crucial in stability and bifurcation analyses, since it is practically impossible to perform these tasks directly on the full model for complex configurations. In this article, we apply the proper orthogonal decomposition (POD) method, first discussed by Lumley [1] in the context of turbulent isothermal flows, to transitional buoyancy-induced flows. This decomposition leads naturally to low-dimensional representations and systematically identifies coherent structures. Identification of the most energetic eigenmodes enables us to compress the data by retaining a small number of such modes that capture most of the flow energy. In mathematical terms, POD is a way of representing fluctuating fields by orthonormal sets of deterministic functions or modes.

Berkooz et al. [2] review the important aspects in applying POD to the analysis of turbulent flows. Sirovich [3] proposed the method of snapshots as an

Received 29 January 1996; accepted 8 March 1997.
This work was partially supported by NASA/LeRC under contract NAG3-1632.
Address correspondence to Professor A. Liakopoulos, Packard Lab. No. 19, Department of Mechanical Engineering, Lehigh University, Bethlehem, Pennsylvania, 18015-3085, USA. E-mail: a103@lehigh.edu

Numerical Heat Transfer, Part A, 32:51–62, 1997

1040–7782/97 $12.00 + .00

NOMENCLATURE

a_i	expansion coefficients for velocity	$\mathbf{V}$	velocity vector
A_c	heat source dimensionless length	x, y	Cartesian coordinates
A_y	aspect ratio of the computational domain	X, Y	nondimensional Cartesian coordinates
		α	thermal diffusivity
b_i	expansion coefficients for temperature	β	thermal expansion coefficient
g	gravitational acceleration	Θ	nondimensional temperature
Gr	Grashof number	$\overline{\Theta}$	dimensionless time-averaged temperature
h	computational domain height		
k	thermal conductivity of the fluid	Θ_b^*	dimensionless reference temperature
l	channel width	ν	kinematic viscosity
l_c	heat source length	ρ	density
p	pressure	ϕ_u, ϕ_v	components of the velocity empirical eigenfunction
P	nondimensional pressure		
Pr	Prandtl number	ψ	temperature empirical eigenfunction
q''	dissipated heat flux		
Ra	Rayleigh number	**Subscript**	
t	time		
t^*	nondimensional time		
T	temperature	b	reference value
u, v	velocity components		
U, V	nondimensional velocity components	**Superscript**	
$\overline{U}, \overline{V}$	nondimensional time-averaged velocity components	′	fluctuation quantities

efficient way of extracting empirical eigenfunctions from large data sets and applied it to the analysis of turbulent thermal convection in closed systems [4]. Deane et al. [5] applied POD to complex geometry flows in the transitional regime. Sahan et al. [6, 7] also studied transitional flow and heat transfer in a periodically grooved channel, while Liakopoulos et al. [8] reported low-dimensional descriptions of buoyancy-induced flow in a differentially heated cavity. Zero Prandtl number free convection in a vertical channel with discrete heaters is discussed in Ref. [9].

Convective air cooling is an effective mode of heat transfer for many low-heat-flux applications. Air cooling by natural convection finds many applications in communications switching devices, avionics packages, electronic test equipment, consumer electronics, and low-end computer packages [10]. Many investigations of free convection in enclosures and channels have been performed. For a review of relevant publications, see Peterson and Ortega [10] and Incropera [11]. Liakopoulos et al. [12] performed numerical investigations of two-dimensional thermally driven convective flows in cavities and vertical channels for Pr = 0.71 and a wide range of values of Gr. In this article we present a low-dimensional representation of some buoyancy-driven flows discussed by Liakopoulos et al. [12].

In the present study the snapshot version of POD is used to extract the coherent structures and to obtain a low-order dynamical model of a transitional flow in a vertical channel. We consider two-dimensional natural convection flow due to periodically spaced heat sources of uniform heat flux. The heat sources are flush mounted on the left vertical wall. The right vertical wall is kept isothermal.

We apply the POD method to data obtained by numerically solving the full governing equations. Using the computed eigenfunctions, we are able to reconstruct the original flow and temperature fields in an optimal way. It is found that almost all the flow energy is captured by the first six modes. A low-dimensional set of nonlinear ordinary differential equations that describes the dynamics of the flow and temperature fields is also derived. It is found that low-order models based on retaining at least four eigenmodes for each field result in stable, self-sustained oscillations with correct amplitude.

MATHEMATICAL FORMULATION AND MODEL REDUCTION

Full Model

We consider two-dimensional incompressible time-dependent buoyancy-driven flow. Neglecting viscous dissipation and energy generation, the governing partial differential equations for a Boussinesq fluid can be written in dimensionless form as follows.

Conservation of mass

$$\frac{\partial U}{\partial X} + \frac{\partial V}{\partial Y} = 0 \tag{1}$$

X momentum

$$\frac{\partial U}{\partial t^*} + U\frac{\partial U}{\partial X} + V\frac{\partial U}{\partial Y} = -\frac{\partial P}{\partial X} + \mathrm{Pr}\left(\frac{\partial^2 U}{\partial X^2} + \frac{\partial^2 U}{\partial Y^2}\right) \tag{2}$$

Y momentum

$$\frac{\partial V}{\partial t^*} + U\frac{\partial V}{\partial X} + V\frac{\partial V}{\partial Y} = -\frac{\partial P}{\partial Y} + \mathrm{Pr}\,\mathrm{Ra}\,\Theta + \mathrm{Pr}\left(\frac{\partial^2 V}{\partial X^2} + \frac{\partial^2 V}{\partial Y^2}\right) \tag{3}$$

Energy equation

$$\frac{\partial \Theta}{\partial t^*} + U\frac{\partial \Theta}{\partial X} + V\frac{\partial \Theta}{\partial Y} = \left(\frac{\partial^2 \Theta}{\partial X^2} + \frac{\partial^2 \Theta}{\partial Y^2}\right) \tag{4}$$

In the above equations, the dimensionless variables have been defined as follows:

$$(X, Y) = \frac{1}{l}(x, y) \tag{5}$$

$$t^* = \frac{\alpha}{l^2}t \tag{6}$$

$$(U, V) = \frac{l}{\alpha}(u, v) \tag{7}$$

$$P = \frac{l^2}{\rho_0 \alpha^2} p \tag{8}$$

$$\Theta = \frac{k}{q'' l}(T - T_b) \tag{9}$$

In general, lower case letters denote dimensional variables. However, note that the dimensional temperature is denoted by T and the dimensionless time is denoted by t^*. In the above, (x, y) and (u, v) denote the Cartesian coordinates and velocity components, respectively, p is the pressure relative to the background hydrostatic distribution, l is the width of the vertical channel (see Figure 1), k is the thermal conductivity of the fluid, α is the thermal diffusivity, ν is the kinematic viscosity, β is the thermal expansion coefficient, g is the gravitational acceleration, ρ_0 is the reference density, T_b is the reference temperature, and q'' denotes the uniform input heat flux of the heat sources. In Eqs. (2) and (3), $\mathrm{Pr} = \nu/\alpha$ denotes the Prandtl number and $\mathrm{Ra} = \mathrm{Gr}\,\mathrm{Pr} = \beta g q'' l^4/\nu\alpha k$ denotes the Rayleigh number.

The boundary conditions for the configuration considered in this study (Figure 1) are

$$\mathbf{V}(X, Y, t^*) = \mathbf{0} \tag{10}$$

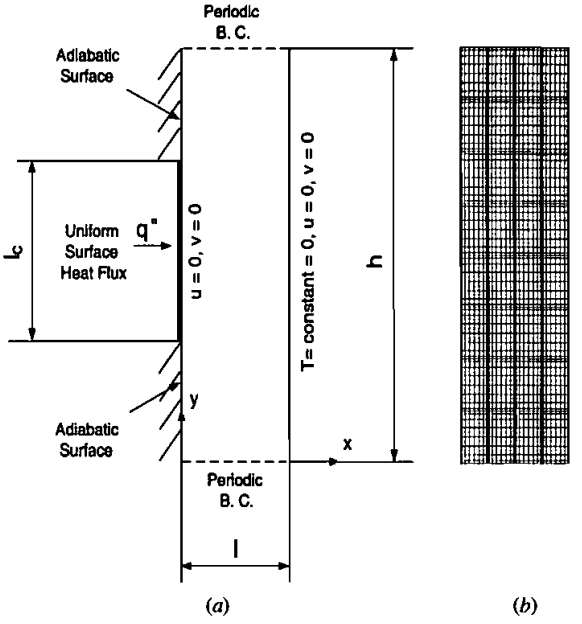

Figure 1. (*a*) Computational domain and boundary conditions. $A_c = l_c/l = 2$ and $A_y = h/l = 4$. (*b*) Computational mesh: 32 spectral elements each with 9×9 collocation points.

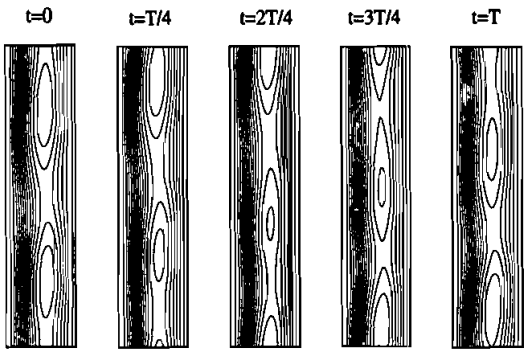

Figure 2. Instantaneous streamlines (Pr = 0.71, Gr = 22,500, $\Theta_b^* = 0.226$). T is period of oscillation.

at solid walls,

$$\mathbf{V}(X, 0, t^*) = \mathbf{V}(X, A_y, t^*) \tag{11}$$

$$\frac{\partial \Theta}{\partial X} = \begin{cases} -1 & \text{on } \partial\Omega_C \\ 0 & \text{on } \partial\Omega_A \end{cases} \tag{12}$$

$$\Theta = \frac{k}{q'' l}(T_C - T_b) = -\Theta_b^* = \text{const} \qquad \text{on } \partial\Omega_T \tag{13}$$

$$\Theta(X, 0, t^*) = \Theta(X, A_y, t^*) \tag{14}$$

where $A_y = h/l$, $\partial\Omega_C$ denotes the uniform heat flux surface, $\partial\Omega_A$ denotes the adiabatic surface, and $\partial\Omega_T$ denotes the uniform temperature surface (see Figure 1). Note that periodic boundary conditions are imposed in the y direction, so that the model is valid far from the channel entrance.

The governing equations, Eqs. (1)–(4), with boundary conditions Eqs. (10)–(14) are solved using a spectral element method [13]. Spectral element methods are high-order weighted-residual techniques that are able to represent relatively complex geometries while retaining the high-resolution properties of the spectral methods [14]. Implementation of the numerical method is based on a computer code, Nekton, developed by Patera and his co-workers [15] to simulate steady and unsteady incompressible fluid flow, heat, and mass transfer. In our simulations, 32 spectral elements are used. Numerical solutions were obtained for order of interpolants, $N = 4, 6, 8, 10$, and 12 in order to achieve convergence. The error due to spatial resolution is negligible for $N \geqslant 10$. Instantaneous streamlines and isotherms are shown in Figures 2 and 3 for Pr = 0.71, Gr = 22,500, $\Theta_b^* = 0.226$, $A_c = l_c/l = 2$, and $A_y = h/l = 4$.

Low-Order Models

In applying the POD methodology, the time-dependent data obtained through direct numerical simulation are decomposed into time-averaged ($\overline{U}$, $\overline{V}$, and $\overline{\Theta}$) and

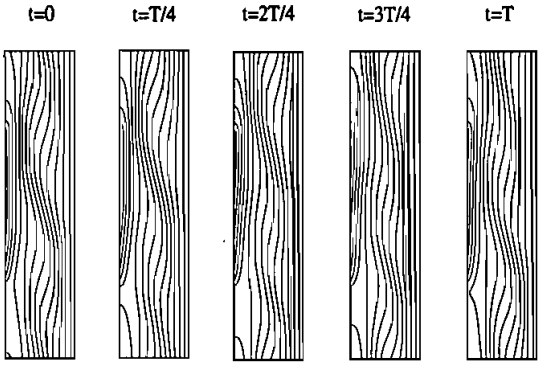

Figure 3. Instantaneous isotherms (Pr = 0.71, Gr = 22,500, $\Theta_b^* = 0.226$). T is period of oscillation.

time-varying (U', V', and Θ') parts:

$$U(X,Y,t^*) = \bar{U}(X,Y) + U'(X,Y,t^*) \tag{15}$$

$$V(X,Y,t^*) = \bar{V}(X,Y) + V'(X,Y,t^*) \tag{16}$$

$$\Theta(X,Y,t^*) = \bar{\Theta}(X,Y) + \Theta'(X,Y,t^*) \tag{17}$$

The time-averaged values are obtained as simple arithmetic means of M snapshots of the velocity and temperature fields. The empirical eigenfunctions are constructed by an appropriate superposition of the time-varying parts of the field variables, i.e.,

$$\phi_{uk}(X,Y) = \sum_{i=1}^{M} A_{ki} U_i'(X,Y,t_i^*) \tag{18}$$

$$\phi_{uk}(X,Y) = \sum_{i=1}^{M} A_{ki} V_i'(X,Y,t_i^*) \tag{19}$$

$$\psi_k(X,Y) = \sum_{i=1}^{M} A_{ki} \Theta_i'(X,Y,t_i^*) \tag{20}$$

where A_k are the eigenvectors of the matrix eigenvalue problem

$$CA = \lambda A \tag{21}$$

The matrix C is given by

$$C_{mn} = \frac{1}{M} \int_\Omega F_{mn}(X,Y,t^*)\, d\Omega \tag{22}$$

where

$$F_{mn} = U_m'(X,Y,t^*)U_n'(X,Y,t^*) + V_m'(X,Y,t^*)V_n'(X,Y,t^*) \tag{23}$$

for the velocity field, and

$$F_{mn} = \Theta_m'(X,Y,t^*)\Theta_n'(X,Y,t^*) \tag{24}$$

for the temperature field. The resulting eigenfunctions are orthogonal and satisfy the boundary conditions of the problem. Furthermore, if the flow is incompressible, the velocity empirical eigenfunctions are divergence free. After normalizing the eigenfunctions, we expand the time-varying parts of the velocity and temperature fields in terms of the eigenfunctions, i.e.,

$$U'(X,Y,t^*) = \sum_{k=1}^{M_1} a_k(t)\phi_{uk}(X,Y) \tag{25}$$

$$V'(X,Y,t^*) = \sum_{k=1}^{M_1} a_k(t)\phi_{vk}(X,Y) \tag{26}$$

$$\Theta'(X,Y,t^*) = \sum_{k=1}^{M_1} b_k(t)\psi_k(X,Y) \tag{27}$$

where ϕ_{uk} and ϕ_{vk} denote the x and y components of the kth velocity eigenfunction, respectively, and ψ_k denotes the kth temperature eigenfunction. In general, $M_1 \ll M$ and $M_2 \ll M$ in order to obtain a low-order model.

Substituting Eqs. (25)–(27) into the governing equations, Eqs. (1)–(4), applying Galerkin's method, and using the orthonormality property of the empirical eigenfunctions, we obtain a system of nonlinear ordinary differential equations (ODEs) for the expansion coefficients of the form

$$\frac{da_k}{dt^*} = A_k + \mathrm{Pr}\, B_k + \mathrm{Pr\,Ra}\, C_k + \sum_{i=1}^{M_1} D_{ki}a_i - \mathrm{Pr} \sum_{i=1}^{M_1} E_{ki}a_i + \mathrm{Pr\,Ra} \sum_{i=1}^{M_2} F_{ki}b_i + \sum_{i=1}^{M_1}\sum_{j=1}^{M_1} G_{kij}a_ia_j \tag{28}$$

$$\frac{db_k}{dt^*} = H_k + \sum_{i=1}^{M_1} K_{ki}a_i + \sum_{i=1}^{M_2} L_{ki}b_i + \sum_{i=1}^{M_1}\sum_{j=1}^{M_2} M_{kij}a_ib_j \tag{29}$$

The coefficients appearing in the above equations arise from the various inner products among eigenmodes and/or mean flow and temperature. Equations (28) and (29) are integrated using a fourth-order Runge-Kutta solver.

RESULTS AND DISCUSSION

We present results for a 12-equation model obtained by retaining the six most energetic eigenfunctions for each field. As input data, we use 20 snapshots obtained by solving the full model equations for Gr = 22,500, Pr = 0.71, and $\Theta_b^* = 0.226$. $M = 20$ is found to be adequate. Similar results are obtained for $M = 30$, 40, and 50.

The normalized eigenvalues of the first eight modes are given in Table 1 for velocity and temperature. The eigenvalues are ordered from the most energetic to the least energetic modes. The first two eigenvalues constitute most of the energy of the system. The eigenvalues occur in pairs of similar magnitude. As found in the case of flow in a grooved channel [5–7], an exchange of phase between members of

Table 1. Eigenvalues of the eight most energetic modes and their respective contributions to the total flow and temperature fluctuation "energy"

Mode	Normalized eigenvalue	Energy, %
Velocity modes		
1	0.5240	52.40
2	0.4725	99.64
3	0.0019	99.83
4	0.0015	99.98
5	8.06×10^{-6}	99.99
6	4.55×10^{-6}	99.99
7	1.09×10^{-7}	99.99
8	5.00×10^{-8}	99.99
Temperature modes		
1	0.5225	52.25
2	0.4707	99.32
3	0.0035	99.68
4	0.0031	99.98
5	4.84×10^{-5}	99.99
6	3.71×10^{-5}	99.99
7	5.26×10^{-6}	99.99
8	5.23×10^{-7}	99.99

Note that percent energy shows the cumulative energy of the modes.

the pairs is observed. Table 1 reveals that the first two velocity modes show strong dominance over other modes and capture 99.64% of the kinetic energy of the velocity fluctuation field. The cumulative contribution from the first four modes reaches the energy level of 99.98%, and the first six modes capture practically the total energy of the flow. Similar trends are observed for the temperature modes in Table 1. The contribution from the first two temperature modes reaches 99.32% of the total "energy," the first four modes retain 99.98% of the total energy, while the first six temperature modes represent almost the whole energy. Thus the first six eigenmodes should be able to capture the structure of the field and its dynamics. These six modes are used as basis functions in the truncated series expansions, Eqs. (25)–(27), and they are used to reconstruct the flow and temperature fields.

The first six empirical eigenfunctions for velocity and temperature are shown in Figures 4 and 5, respectively. The two most energetic modes capture the large-scale features of the flow, while higher modes contain smaller scale features. Furthermore, it can be seen that, within the same pair, the spatial structures are characterized by a phase shift of approximately $\pi/2$ in the streamwise direction. This behavior has also been observed in the studies of Deane et al. [5], Sahan et al. [6, 7], and Gunes et al. [9]. Similar observations can be made for the temperature eigenmodes shown in Figure 5. The first two eigenfunctions are approximately phase-shifted versions of each other. The same relation is also true for the remaining pairs of eigenfunctions.

Figure 6 shows the amplitudes of the eigenmodes [expansion coefficients in Eqs. (25)–(27)] obtained by direct projection of the input velocity and temperature

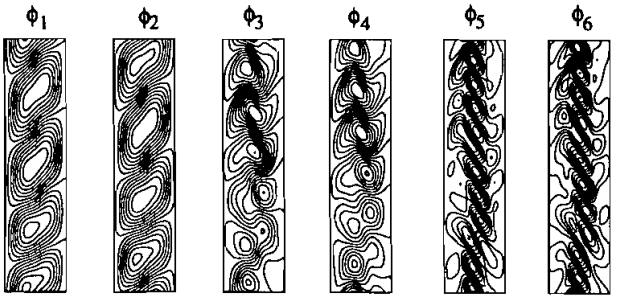

Figure 4. Velocity empirical eigenfunctions (streamlines), Pr = 0.71, Gr = 22,500.

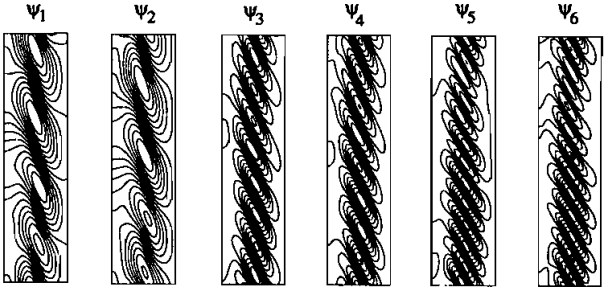

Figure 5. Temperature eigenfunctions (isotherms), Pr = 0.71, Gr = 22,500.

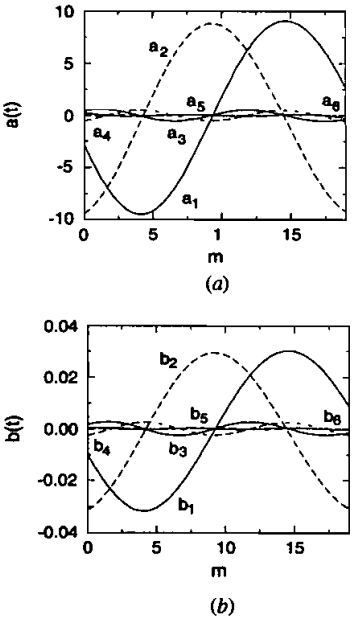

Figure 6. Amplitudes of the six most energetic modes from direct projection. (*a*) Velocity modes. (*b*) Temperature modes. *Pr* = 0.71, *Gr* = 22,500.

data. Comparisons of expansion coefficients obtained by direct projection of the full model data on the computed eigenfunctions and by the low-order model are shown in Figures 7 and 8. Amplitudes a_1, a_2, b_1, and b_2 are in a very good agreement. Higher modes show also quite good agreement, but in general, predictions based on the 12-equation model exhibit oscillations of slightly larger amplitude than those calculated by direct projection. It should be noted that similar results are obtained by using an eight-equation model. Further reduction of the dimensionality of the system of ODEs leads to models that are incapable of predicting correctly the dynamical behavior of the flow system.

CONCLUDING REMARKS

Two-dimensional buoyancy-driven flow in a vertical channel with discrete heaters has been numerically investigated. A time-dependent solution in the transitional regime has been analyzed by the method of empirical eigenfunctions

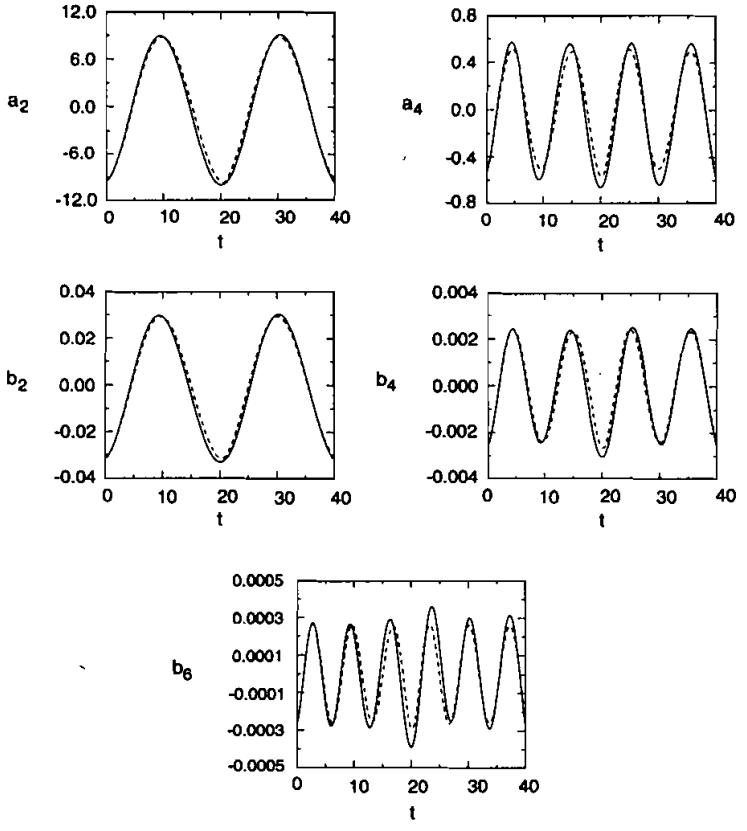

Figure 7. Amplitudes of the velocity and temperature modes, Pr = 0.71, Gr = 22,500 (dashed line, direct projection (full model); solid line, low-order model).

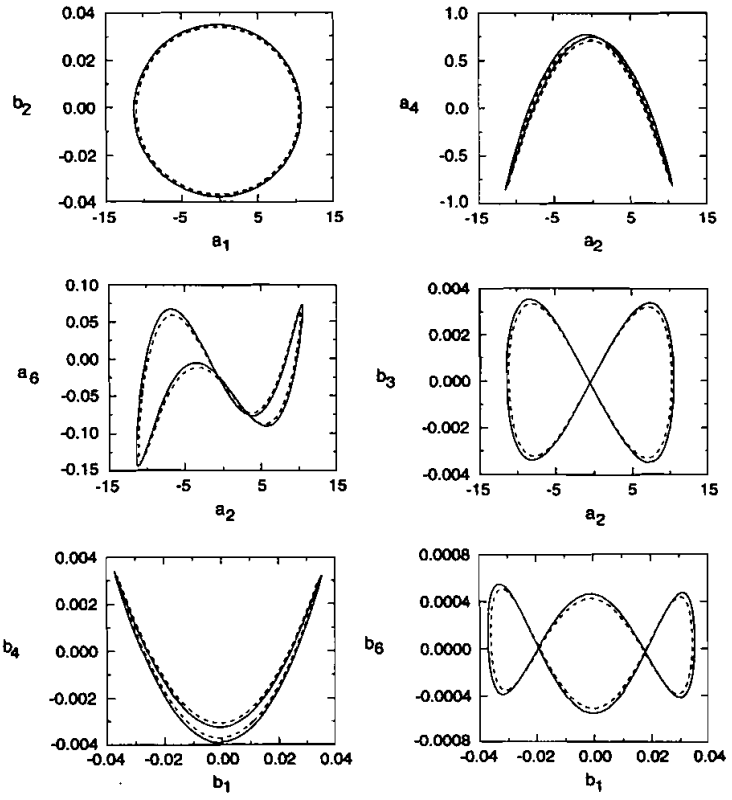

Figure 8. Phase portraits of velocity and temperature mode amplitudes, Pr = 0.71, Gr = 22,500 (dashed line, direct projection (full model); solid line, low-order model).

(POD) to reveal the coherent structures of the flow. The eigenfunctions associated with the largest eigenvalues are the modes that explain the dynamical behavior of the flow. A set of ordinary differential equations was also obtained for the time-dependent amplitudes of the eigenfunctions.

It is found that the first six modes of each field capture nearly all the energy. These modes occur in pairs and are phase shifted. At least four modes are required to predict stable, self-sustained oscillations in time. Retaining only four modes reduces the order of the model and facilitates stability and bifurcation studies.

The validity of the 12-equation model is confirmed by comparing full simulation results and reduced model predictions. It is found that the first two mode amplitudes are in very good agreement. Higher modes are also overall well predicted. However, the 12-equation model predicts mode amplitudes for the higher modes that are slightly larger than those obtained by direct projection of the full model data on the computed eigenfunctions.

REFERENCES

1. J. L. Lumley, The Structure of Inhomogeneous Turbulence, in A. M. Yaglom and V. I. Tatarski (eds.), *Atmospheric Turbulence and Radio Wave Propagation*, pp. 166–178, Nauko, Moscow, 1967.
2. G. Berkooz, P. Holmes, and J. L. Lumley, The Proper Orthogonal Decomposition in the Analysis of Turbulent Flows, *Annu. Rev. Fluid Mech.*, vol. 25, pp. 539–575, 1993.
3. L. Sirovich, Turbulence and the Dynamics of Coherent Structures: I-III, *Q. J. Appl. Math.*, vol. 45, no. 3, pp. 561–590, 1987.
4. L. Sirovich, M. Maxey, and H. Tarman, An Eigenfunction Analysis of Turbulent Thermal Convection, in J. C. Andre, J. Cousteix, F. Durst, et al. (eds.), *Turbulent Shear Flows 6*, pp. 68–77, Springer, New York, 1989.
5. A. E. Deane, I. G. Kevrekidis, G. E. Karniadakis, and S. A. Orszag, Low Dimensional Models for Complex Geometry Flows: Application to Grooved Channels and Circular Cylinders, *Phys. Fluids A*, vol. 3, no. 10, pp. 2337–2354, 1991.
6. R. A. Sahan, H. Gunes, and A. Liakopoulos, Low-Dimensional Models for Coupled Momentum and Energy Transport Problems, in C. Amon (ed.), *Cooling and Thermal Design of Electronic Systems*, HTD-vol. 319/EEP-vol. 15, pp. 1–15, ASME, New York, 1995.
7. R. A. Sahan, A. Liakopoulos, and H. Gunes, Reduced Dynamical Models of Nonisothermal Transitional Grooved Channel Flow, *Phys. Fluids*, vol. 9, no. 3, pp. 551–565, 1997.
8. A. Liakopoulos, P. A. Blythe, and H. Gunes, A Reduced Dynamical Model of Convective Flows in Tall Laterally Heated Cavities, *Proc. R. Soc. London Ser. A*, vol. 453, pp. 663–672, 1997.
9. H. Gunes, A. Liakopoulos, and R. A. Sahan, Low-Dimensional Description of Oscillatory Thermal Convection: The Small Prandtl Number Limit, *Theoret. Comput. Fluid Dyn.*, in press.
10. G. P. Peterson and A. Ortega, Thermal Control of Electronic Equipment and Devices, *Adv. Heat Transfer*, vol. 20, pp. 181–314, 1990.
11. F. P. Incropera, Convection Heat Transfer in Electronic Equipment Cooling, *J. Heat Transfer*, vol. 110, pp. 1097–1111, 1988.
12. A. Liakopoulos, P. A. Blythe, and P. G. Simpkins, Convective Flows in Tall Cavities, in A. F. Emery (ed.), *Simulation and Numerical Methods in Heat Transfer*, HTD-vol. 157, pp. 81–87, ASME, New York, 1990.
13. A. T. Patera, A Spectral Element Method for Fluid Dynamics: Laminar Flow in a Channel Expansion, *J. Comput. Phys.*, vol. 54, pp. 468–488, 1984.
14. G. E. Karniadakis, Spectral Element Simulation of Laminar and Turbulent Flows in Complex Geometries, *Appl. Numer. Math.*, vol. 6, nos. 1-2, pp. 85–105, 1989.
15. Nektonics Inc., *Nekton Users Manual*, Release 2.9, 1994.